Plasmonic effects on strong exciton-photon coupling in metal-insulator-metal microcavities

Shinji Hayashi,* Yuta Ishigaki, and Minoru Fujii

Department of Electrical and Electronic Engineering, Graduate School of Engineering, Kobe University, Rokko, Nada, 657-8501 Kobe, Japan

(Received 10 April 2012; revised manuscript received 21 May 2012; published 5 July 2012)

Metal-insulator-metal (MIM) microcavities consisting of a layer of polyvinyl alcohol doped and undoped with cyanine dye molecules were prepared and their reflection and transmission spectra were measured. In the doped-MIM microcavity, dispersion curves determined from the reflection data clearly showed the anticrossing behavior arising from the strong coupling between excitons in the dye molecules and photonic modes supported by the MIM microcavity. The experimental dispersion curves could be well reproduced by a standard expression of the coupled mode dispersions by appropriately taking into account the plasmonic nature of the transverse magnetic mode supported by the MIM microcavity. A large splitting between the transverse electric and transverse magnetic modes in the upper branch of the coupled modes can also be well explained by the plasmonic effects.

DOI: 10.1103/PhysRevB.86.045408 PACS number(s): 73.21.Ac, 78.40.Kc, 78.40.Me, 78.67.Pt

I. INTRODUCTION

During the past two decades, strong coupling between excitons and photons in planar microcavities has been the subject of extensive experimental and theoretical studies.[1–6] The first demonstration of strong coupling in solid state physics, which is an analog of strong coupling of atomic states with cavity photon modes, has been made by Weisbuch *et al.*[7] in a semiconductor quantum microcavity. They prepared a Fabry-Pérot microcavity consisting of GaAs quantum wells imbedded between two distributed Bragg reflectors (DBRs). In such microcavities, when the energy of the confined photon mode is tuned to match that of the exciton in the quantum wells, strong exciton-photon coupling takes place, generating so-called cavity polaritons that are characterized by a doublet of dispersion curves separated by the Rabi splitting energy. For microcavities containing active layers of inorganic semiconductors that support Wannier-Mott excitons, Rabi splitting energies ranging from 5 to 10 meV were reported.[1,3,4] For microcavities containing organic semiconductors such as *J* aggregates of dye molecules that support Frenkel excitons with large oscillator strengths, Rabi splitting energies larger than 100 meV were observed.[5,8,9]

The strong exciton-photon coupling has also been studied for microcavities in which DBRs are replaced by metal mirrors.[10–14] An advantage of using metal mirrors is that they serve as electrodes and allow electric excitation of the cavity polaritons.[11,14] Since the penetration depth of optical fields into metal mirrors is smaller than that into DBRs, the photon confinement in the metal-mirror microcavity is stronger than that in the DBR microcavity. This leads to larger Rabi splitting energies for metal-mirror microcavities, as experimentally demonstrated by Hobson *et al.*[10] When the Rabi splitting energy is as high as a significant fraction of the transition energy of the active material, the light-matter coupling enters into the so-called ultrastrong-coupling regime, which is currently the subject of intensive theoretical and experimental studies. In this regime, a standard theoretical expression of the Rabi splitting energy for the strong-coupling case is no more valid and the appearance of new phenomena such as the generation of correlated photon pairs has been predicted theoretically.[15–17] The ultrastrong-coupling regime has been achieved so far by intersubband transitions of inorganic semiconductor multiple quantum wells in terahertz frequency regions[17–19] and also by superconducting quantum circuits in gigahertz frequency regions.[20] Very recently, Schwartz *et al.*[13] have demonstrated a Rabi splitting energy as large as 700 meV in the visible region for spiropyran molecules embedded in Ag-mirror microcavities. This large Rabi splitting energy is 32% of the molecular transition energy and their samples are thought to work amply in the ultrastrong-coupling regime.

Strong interaction between surface polaritons supported by solid surfaces and elementary excitations of thin overlayers or transition layers on the surfaces has also been the subject of extensive studied for a long time. Agranovich *et al.*[21–23] theoretically predicted that the dispersion curves of surface polaritons are split and exhibit anticrossing behaviors, when the energy of the elementary excitation of the overlayer is located in the energy range of the surface polaritons. Yakovlev *et al.*[24] reported splitting of reflection dips in attenuated-total-reflection spectra of saphire (Al_2O_3) and rutile (TiO_2) substrates coated with thin films of LiF. The splitting of the reflection dips is the manifestation of the strong interaction between surface phonon polaritons at the saphire and rutile surfaces with the longitudinal optical phonon in the LiF thin overlayers. Lopez-Rios *et al.*[25] reported the splitting of the dispersion curve of surface plasmon polaritons (SPPs) supported by Al surfaces coated with thin Ag overlayers. Experiments made by Pockrand *et al.*[26] also demonstrated the splitting of the dispersion curve of SPPs supported by Ag surfaces strongly interacting with molecular excitons in dye overlayers. In recent years, strong coupling of SPPs with excitons of organic materials has attracted renewed interest[27–31] because of the rapid growth of the research field of *plasmonics*. Bellesa *et al.*[27] performed reflection and photoluminescence measurements for a system of an Ag film coated by a polymer layer containing *J* aggregates of cyanine dye molecules. They clearly demonstrated the anticrossing behavior of the dispersion curves and analyzed their results by using a standard expression of strong exciton-photon coupling commonly used for microcavities. Similar strong coupling with SPPs are reported not only for excitons in organic materials,[28,29,31] but also for those in inorganic materials such as CdSe quantum dots.[30] Strong coupling between excitons and localized surface plasmons supported by metallic nanostructures is currently the subject of intensive studies.[32–34]

SPPs supported by metal-insulator-metal (MIM) structures, which are nothing but the metal-mirror microcavities, have long been the subject of intensive theoretical and experimental studies.[35–41] A salient plasmonic feature in the MIM structures with thin enough insulator layers is the coupling of SPP modes at two insulator-metal interfaces resulting in symmetric SPP (S-SPP) and antisymmetric SPP (AS-SPP) modes. This feature was theoretically predicted by Economou[35] early in 1969. Since these modes are of plasmonic origin, they are transverse magnetic (TM) modes. The AS-SPP mode is a nonradiative mode with a waveguide mode character and has potential applications in the field of plasmonic waveguides.[38,39,42] The S-SPP mode has a dispersion curve extending from the radiative to nonradiative regions. When the metal mirrors are thin enough, the radiative part of the S-SPP mode can couple directly with light outside the MIM structures and plays important roles in determining optical properties of the structures. Resonant light transmission mediated by the S-SPP mode has been observed by several authors.[43,44] Hayashi *et al.*[45] have demonstrated that light emission from an emitting layer embedded in the insulator layer can be enhanced when the emission is mediated by the S-SPP mode. Very recently, in analyzing mode structures of a quantum cascade laser, Bogdanov and Suris[46] stressed the importance of plasmonic nature of the modes supported by the MIM structure, while Litinskaya and Agranovich[47] theoretically predicted realization of polariton trap in a MIM structure by using a minimum appearing in the nonradiative part of the dispersion curve of S-SPP mode.

In spite of a lot of studies on the SPPs supported by the MIM structure, as far as the present authors know, no attention has been payed on the plasmonic nature of the TM modes in analyzing previous experimental results of the strong exciton-photon coupling in the metal-mirror microcavities.[10–14] In Refs. 10, 11, and 13, authors reported experimental data only for *s*-polarized light and no discussion is made on the TM-coupled mode. While in Refs. 12 and 14, the data for both the *s*- and *p*-polarized light are reported, but the discussions were made on the basis of the penetration depth of optical fields and phase shift[48,49] in the same way as those for dielectric-mirror microcavities.[1–3,5] In particular, Oda *et al.*[12] mentioned about a difficulty in obtaining a reasonable theoretical fit to their experimental TM branch of the coupled modes by using a standard expression of photonic modes in DBR microcavities. The difficulty seems to arise from the neglect of the plasmonic nature of the TM mode supported by the MIM microcavity.

In this paper, we present results of reflection and transmission measurements performed with *s*- and *p*-polarized light for MIM structures containing an insulator layer doped and undoped with *J* aggregates of cyanine dye molecules. We focus our attention on the role played by the SPP mode in the strong exciton-photon coupling. From the results of the undoped-MIM structure, we identify the transverse electric (TE) and TM modes supported by the structure. Based on the identification, the strong coupling between excitons in the *J* aggregates with the TE and TM modes is discussed. We show that dispersion curves of the TM coupled modes can be well explained without any difficulty by using the dispersion of the S-SPP mode supported by the MIM structure. The large TE-TM polarization splitting observed can also be well explained by the plasmonic nature of the S-SPP mode. This paper is organized as follows. In Sec. II, experimental procedures are described. In Sec III, after identifying the photonic modes supported by the undoped-MIM structure, dispersion curves of coupled modes determined for the doped-MIM structure are analyzed on the basis of the photonic modes in the undoped-MIM structure.

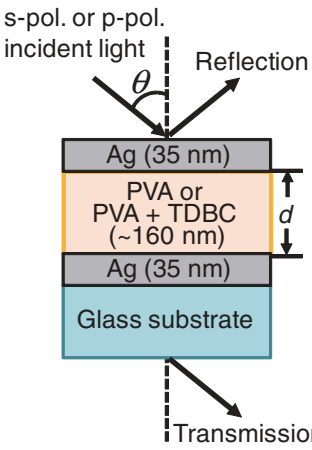

FIG. 1. (Color online) MIM structure prepared.

II. EXPERIMENTAL

The MIM structures prepared are schematically shown in Fig. 1. A 35-nm-thick Ag layer was deposited on a glass substrate by a vacuum evaporation technique. The thickness of the Ag film was monitored by a quartz microbalance during the deposition. The Ag layer is then coated by a layer of polyvinyl alcohol (PVA), which is either doped or undoped with cyanine dye, by using a spin coating method. The MIM structure was completed by depositing a top 35-nm-thick Ag layer. To obtain the dye-doped PVA layer, cyanine dye was dissolved in water and mixed with an aqueous solution of PVA. The cyanine dye used was 5,5′,6,6′-tetrachloro-1-1′-diethyl-3,3′-di(4-sulfobuthyl)-benzimidazolocarbocyanine (TDBC), which is known to form *J* aggregates for concentrations larger than 5×10^{-5} M.[50] The aqueous solution of TDBC (concentration 1.2×10^{-2} M) was mixed with that of PVA (5 wt%) in a proportion of 7 : 10 in volume and spin cast with a rotation speed of ∼2000 rpm. The rotation speed was adjusted to achieve the layer thickness of ∼160 nm. Figure 2 shows a typical absorption spectrum obtained for a TDBC-doped-PVA layer spin cast onto a glass substrate. This spectrum was obtained by a double-beam spectrophotometer with unpolarized light at normal incidence. The absorption spectrum exhibits a strong and sharp peak at 597 nm (2.077 eV) as well as a subsidiary weak peak around 525 nm. The spectrum is very similar to those previously reported for *J* aggregates of TDBC[29,34,50] and confirms the formation of excitons in the *J* aggregates in our samples. As reference samples, MIM structures with undoped-PVA layers were also prepared from the aqueous solution of PVA not containing TDBC. Hereafter, the MIM sample with a TDBC-doped-PVA layer is referred to as doped-MIM sample and that with an undoped-PVA layer as undoped-MIM sample.

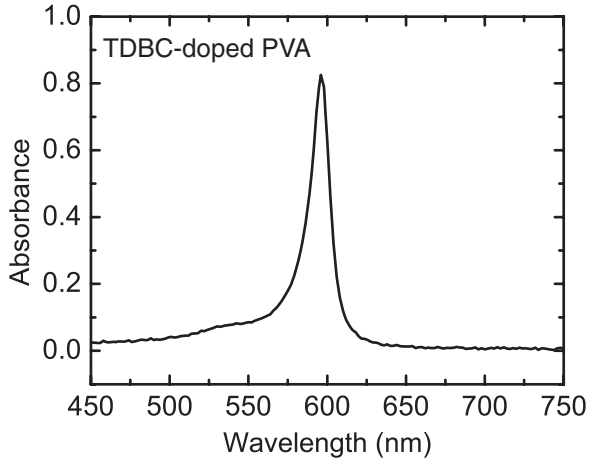

FIG. 2. Typical absorption spectrum of a TDBC-doped PVA film spin cast on a glass substrate.

For the samples prepared, we have performed conventional transmission and reflection measurements for various incident angles θ. Light from a Xe lamp was monochromatized by a single monochromator and polarized by a polarizer. *s*- or *p*-polarized light was incident on the sample mounted on a rotating stage. Reflected and transmitted light was detected by a Si photodiode connected to a lock-in amplifier. Scanning of the incident wavelength and setting of the incident angle were controlled by a computer.

III. RESULTS AND DISCUSSION

A. Dispersion curves of photonic modes in a model MIM microcavity

In order to clarify the photonic modes in the empty microcavity, which may interact with excitons in the doped-MIM microcavity, we present dispersion curves calculated for a model MIM microcavity in Fig. 3. As schematically shown in the inset of the figure, the model cavity is assumed to have a 150 nm-thick insulator layer bounded by two semi-infinite Ag mirrors. As described in detail by Barnes,[36,51] it is possible to obtain dispersion curves of the photonic modes supported by a multilayer system from power dissipation spectra[52] of an oscillating dipole placed in the system. In our calculations, the dipole is located in the middle of the insulator layer and an isotropic orientation is assumed. Literature values of the dielectric function of Ag[53] were used and the dielectric constant of the insulator layer was assumed to be an wavelength-independent constant $\varepsilon = 2.5$. In Fig. 3, whiter regions correspond to higher power dissipation and represent dispersion curves. We see clearly three dispersion branches. By comparing the present results with previous ones,[36,41,45,47] we can assign the highest-energy branch to the lowest-order transverse electric (TE_0) mode. The other two branches are TM modes and can be assigned to the symmetric SPP (S-SPP) and antisymmetric SPP (AS-SPP) modes, as indicated in the figure.

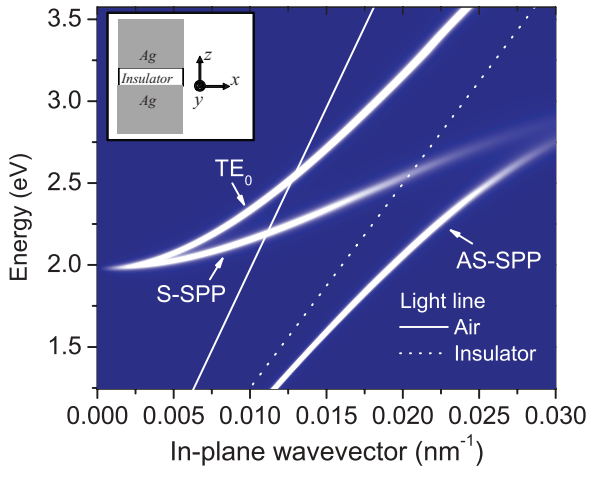

FIG. 3. (Color online) Calculated dispersion curves of photonic modes supported by a model microcavity consisting of a 150-nm thick insulator layer with a dielectric constant $\varepsilon = 2.5$ sandwiched by two semi-infinite Ag mirrors.

As mentioned before, the S-SPP and AS-SPP branches arise from the coupling of two SPP modes at two metal-insulator interfaces. The electric field profiles corresponding to these modes can be found in Refs. 38 and 41. The S-SPP (AS-SPP) mode is characterized by a profile of E_x field (in the coordinate system of the inset of Fig. 3) that is symmetric (antisymmetric) with respect to the middle of the insulator layer. The TE_0 mode is a waveguide mode with a profile of E_y field confined in the microcavity.[38,41] This mode is similar to the photonic modes supported by the empty cavity bounded by DBRs. On the other hand, the S-SPP and AS-SPP modes are of plasmonic origin and their behaviors are different from those of photonic modes in the DBR microcavities. It is important to note that the S-SPP branch is extended from the radiative region (left to the air light line) to the nonradiative region (right to the air light line). As the in-plane wave vector approaches infinity, the S-SPP and AS-SPP branches become flat and approach a horizontal line. When one or both of the Ag mirrors are thin enough, the S-SPP mode in the radiative region can couple directly with light outside the cavity and plays important roles in determining the optical properties of the cavity, such as the resonant light transmission[54] and light emission from light emitters embedded in the microcavity.[45] It should be noted that the dispersion curve of the TE_0 mode exhibits a parabolic dependence on the in-plane wave vector similar to that of photonic modes in DBR microcavities. In contrast to this, the dispersion curve of the S-SPP mode deviates from the parabolic behavior and tends to be flat for large values of the in-plane wave vector. It is well known that the photon energy of the degenerate TE_0 and S-SPP modes at zero in-plane wave vector increases with decreasing the thickness of the insulator layer. Therefore, in strong-coupling experiments with MIM microcavities, the detuning between photonic modes and excitonic transitions can easily be controlled by changing the insulator thickness.

B. Photonic modes supported by an undoped-MIM microcavity

We present here experimental results obtained for an undoped-MIM sample and unambiguously identify the photonic modes supported by the empty microcavity. Figures 4(a) and 4(b) show reflection and transmission spectra obtained with *s*- and *p*-polarized incident light, respectively. To obtain the spectra, the incident angle was varied from 10° to 60°

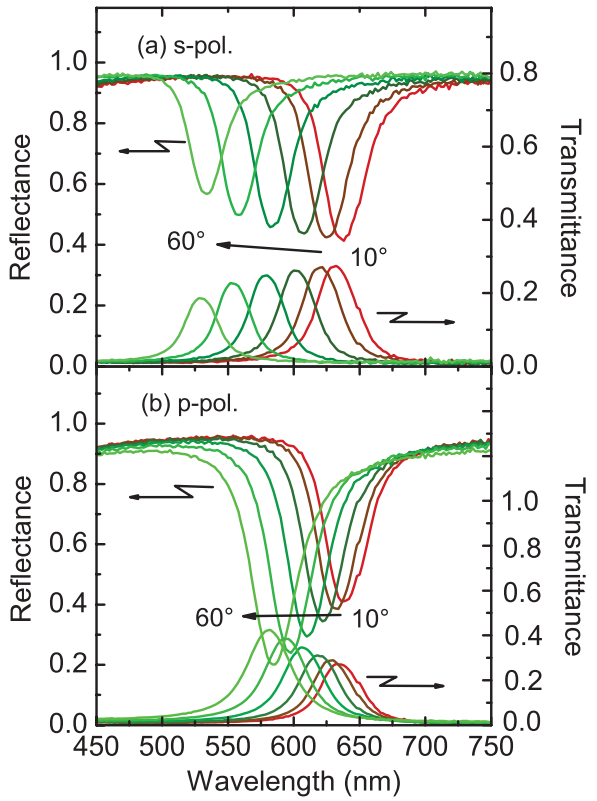

FIG. 4. (Color online) Reflection and transmission spectra obtained for an undoped-MIM sample for various incident angles from 10° to 60° for (a) *s*- and (b) *p*-polarized incident light.

with a step of 10°. The figures demonstrate that for a given incident angle, the undoped-MIM sample exhibits a single reflection dip and a single transmission peak. The dip and peak are located at almost the same wavelength. As the incident angle increases, the dip and peak shift to shorter wavelengths. For small incident angles, the dips and peaks for *s*-polarized incident light [see Fig. 4(a)] are located at nearly the same wavelengths as those for *p*-polarized incident light [see Fig. 4(b)]. However, for the incident angles larger than 30°, the dip and peak for *s*-polarized light are located at considerably shorter wavelengths compared to those for *p*-polarized light. The behaviors of the dips and peaks seen in Figs. 4(a) and 4(b) agree fairly well with results of previous optical studies on MIM structures[37,44,55] and the appearance of the dips and the peaks can be explained in terms of the resonant light transmission mediated by the electromagnetic normal modes or photonic modes supported by the MIM structures.[54]

The photonic modes responsible for the resonant light transmission can be identified by plotting the dispersion relations from the experimental spectra.[54] The dispersion relation of the TE (TM) mode can be obtained from *s*-polarized (*p*-polarized) spectra. We used the reflection spectra to obtain the dispersion relations. The wavelength of the reflection dip for a given incident angle was converted into the photon energy and the in-plane wave vector corresponding to the dip was calculated from the dip wavelength and the incident angle by using a relation $k = \frac{2\pi}{\lambda} \sin\theta$. The experimental dispersion relations obtained are compared with calculated ones in Fig. 5. Open triangles and squares in the figure are experimental

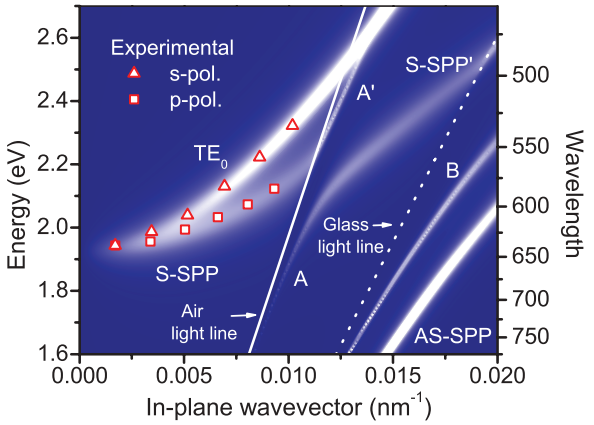

FIG. 5. (Color online) Dispersion curves of photonic modes supported in the undoped-MIM microcavity determined from the reflection spectra for *s*-polarized (open triangles) and *p*-polarized (open squares) incident light. Theoretical dispersion curves obtained from the power dissipation spectra are also shown together with air and glass light lines.

points obtained from *s*- and *p*-polarized reflection spectra, respectively, and the white regions are dispersions of photonic modes obtained from theoretical calculations.

To obtain the theoretical dispersion curves shown in Fig. 5, we assumed the same structure as that of the undoped-MIM sample with the 35 nm-thick Ag mirrors. For the dielectric function of Ag, we used literature values,[53] while for that of the PVA layer, we used values determined from our ellipsometry measurements. Only one free parameter in the calculation was the thickness of the undoped-PVA layer, d. The result shown in Fig. 5 was obtained with $d = 161$ nm. Since the upper and lower Ag layers are thin, the calculated dispersions in Fig. 5 exhibit additional branches denoted A, A′, and B, which are not present in Fig. 3 for the model MIM structure with the semi-infinite Ag layers. The branch B corresponds to an SPP mode localized at the Ag/substrate interface and the branches A and A′ correspond to an SPP mode localized at the Ag/air interface. This branch is split into A and A′ branches because of the hybridization with the S-SPP mode. Similar splitting in the dispersion curves was reported in our previous paper.[45] Although these additional branches appear in the calculated results, the TE_0 and S-SPP branches in the radiative region are very similar to those in Fig. 3. Figure 5 demonstrates that the experimental points obtained from the *s*-polarized spectra agree very well with the dispersion of the TE_0 mode, while those obtained from the the *p*-polarized spectra agree very well with that of the S-SPP mode. It is now very clear that the photonic modes governing the resonant light transmission in the present undoped-MIM sample are TE_0 and S-SPP modes.

C. Coupled modes in a doped-MIM microcavity

We now turn to the discussion of strong coupling in a doped-MIM sample. Figures 6(a) and 6(b) show reflection and transmission spectra of a doped-MIM sample obtained for *s*- and *p*-polarized incident light, respectively. In contrast to the spectra shown in Figs. 4(a) and 4(b) with single dips and peaks, the spectra in Figs. 6(a) and 6(b) exhibit doublets of dips and peaks for each incident angle, which is the

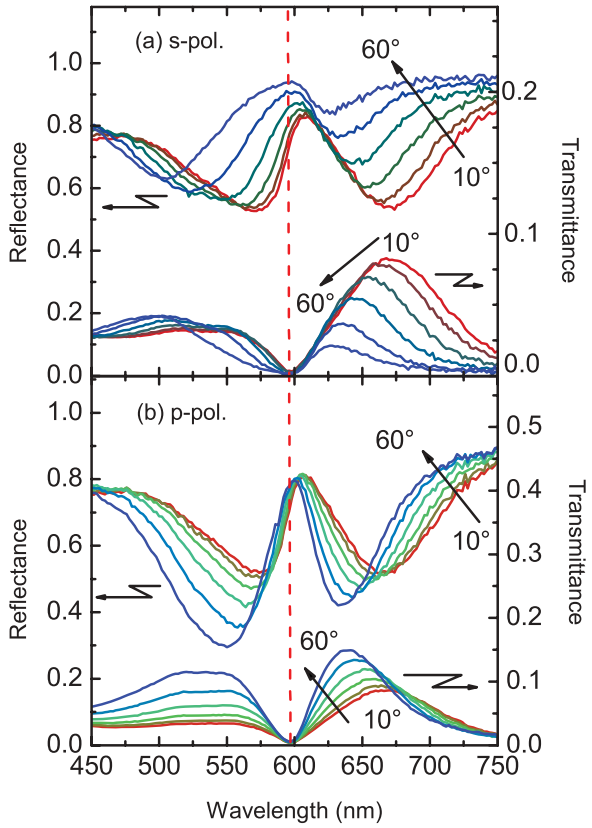

FIG. 6. (Color online) Reflection and transmission spectra obtained for a doped-MIM sample for various incident angles from 10° to 60°. For (a) *s*- and (b) *p*-polarized incident light.

consequence of the strong coupling in the doped-MIM sample. In the transmission spectra, the short-wavelength peak appears to have two components separated by a dip located around 525 nm. However, the position of this dip agrees very well with that of subsidiary absorption peak of TDBC *J* aggregates (see Fig. 2) and consequently, the dip can be attributed to the subsidiary absorption. The short-wavelength peak is thought to be essentially singlet. Since the shift of the doublets as a function of the incident angle is more clearly seen in the reflection spectra, dispersion relations are obtained from the dip positions in the reflection spectra. In Fig. 7, dispersion relations obtained for *s*- and *p*-polarized incident light are presented by filled triangles and squares, respectively. We see a large splitting between the upper and lower branches for both the TE and TM modes. Furthermore, a large polarization splitting in the upper branch, i.e., splitting between the TE and TM modes, can also clearly be seen.

In many previous studies on the strong exciton-photon coupling,[1,5,11,12,27] it was common to determine the energy of Rabi splitting E_{Rabi} by fitting the following theoretical expression of coupled-mode dispersions $E(k)$ to experimental results:

$$E(k) = \frac{E_p(k) + E_{\mathrm{ex}}}{2} \pm \frac{1}{2}\sqrt{[E_p(k) - E_{\mathrm{ex}}]^2 + E_{\mathrm{Rabi}}^2}, \quad (1)$$

where k is the magnitude of the in-plane wave vector, $E_p(k)$ represents the dispersion of uncoupled photonic mode in an empty microcavity and E_{ex} is the energy of an excitonic

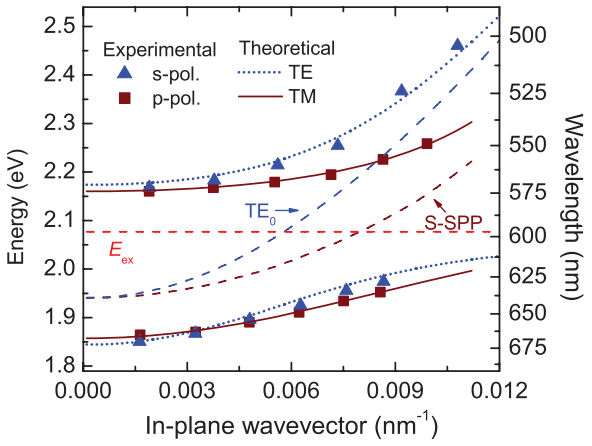

FIG. 7. (Color online) Dispersion curves of the coupled modes determined from reflection data for *s*-polarized light (filled triangles) and for *p*-polarized light (filled squares). The best-fit curves to Eq. (1) in the text are given as dotted lines for TE modes and solid lines for TM modes. The exciton energy and dispersion curves of the TE_0 and S-SPP modes in the empty microcavity obtained from the power dissipation calculations are shown by broken lines.

transition, which is assumed to be independent of k. This expression has been derived on the basis of several theoretical frameworks,[5] such as a quantum mechanical treatment of coupled harmonic oscillators[1] and a classical linear dispersion model.[56] In general, E_{Rabi} depends on both the magnitude and direction of the in-plane wave vector. However, E_{Rabi} was commonly assumed to be a constant independent of the in-plane wave vector.[2] We also performed the fitting by assuming a constant E_{Rabi} and could obtain the best-fit curves presented in Fig. 7 as dotted and solid lines for the TE and TM modes, respectively. In the fitting procedure, we used the exciton energy of $E_{\mathrm{ex}} = 2.077$ eV determined from the absorption spectrum (see Fig. 2). Since the photonic modes in our empty microcavity are the TE_0 and S-SPP modes as identified in the previous subsection, $E_p(k)$ resulting from the calculation of power dissipation spectra was used. Although the results of power dissipation calculation can be displayed in contour plots similar to those in Figs. 3 and 5, in the present fitting procedures, $E_p(k)$ curves were generated by connecting the positions of peaks in the power dissipation spectra. The thickness of the undoped-PVA layer d and the energy of Rabi splitting E_{Rabi} were taken as free parameters in the fitting procedure. The best-fit curves presented in Fig. 7 could be obtained by setting $d = 160$ nm, and $E_{\mathrm{Rabi}} = 300$ and 280 meV for the TE- and TM-coupled modes, respectively. In the figure, the exciton energy and the dispersion relations of the TE_0 and S-SPP modes are also shown as broken lines. We note here that the detuning between the uncoupled photonic modes and the exciton transition in the present sample is 130 meV. Figure 7 demonstrates that the above fitting procedures are successful and reproduce fairly well the experimental dispersions of the coupled modes in the doped-MIM microcavity.

In a previous paper, Oda *et al.*[12] reported experimental results very similar to ours for an MIM cavity consisting of Ag mirrors and an active layer of potassium polyvinyl sulfate containing *J* aggregates of cyanine chloride. In

analyzing their data, they used an equation of the dispersion of photonic modes in empty microcavities frequently used for DBR microcavities.[1,5,56,57] In the equation, the dispersion is expressed as a parabolic function of the magnitude of the in-plane wave vector. By using the parabolic equation together with Eq. (1), they could successfully reproduce the experimental dispersion curve for the TE-coupled mode, but they had a problem to consistently reproduce the dispersion curve for the TM-coupled mode. Their difficulty in analyzing the TM-coupled mode stems from the neglect of the plasmonic nature of the TM modes in the empty MIM microcavity. In fact, the dispersion curve of the S-SPP mode in a MIM microcavity becomes flat and approaches a horizontal line as the in-plane wave vector increases (see Fig. 3). In addition, the hybridization with the SPP mode at the Ag/air interface modifies the dispersion curve (see Fig. 5). Therefore the TM mode in the empty microcavity can not be described by a parabolic function. As far as we know, the plasmonic nature of the TM mode has been discarded so far in analyzing experimental results on the strong coupling in MIM microcavities and discussions[12,14] were made on the basis of the phase shift upon reflection and penetration depth[48,49] in the same way as in DBR microcavities. Figure 7 demonstrates that there is no difficulty in reproducing the dispersions of the coupled mode, when the dispersions of photonic modes in the empty microcavity (TE_0 and S-SPP modes) are properly taken into account.

The energies of Rabi splitting presently obtained are quite large compared to those obtained for microcavities with DBR mirrors containing inorganic excitonic materials.[1,3–5] As has been pointed out already by Hobson *et al.*,[10] one of the reasons for the large Rabi splitting is a large oscillator strength of the excitonic transiton in the organic *J* aggregates, since the Rabi splitting is proportional to the square root of the oscillator strength. Another reason is the strong photon confinement in the metal-metal microcavity caused by smaller field penetration into the metal mirrors. The Rabi splitting obtained for the TE mode is slightly larger than that for the TM mode. This can be explained by the optical anisotropy in the TDBC-doped PVA film caused by a preferential orientation of TDBC *J* aggregates induced during the spin coating process. The effects of the optical anisotropy are discussed in detail in the following subsection.

The TE-TM polarization splitting observed for the upper branch of the coupled modes is extremely large compared to results previously reported for inorganic and organic excitons in DBR microcavities. In previous reports on DBR micorcavities, the branch of the TM mode is located at higher energies than that of the TE mode and the maximum TE-TM splitting reported by Panzarini *et al.*[2] for InGaAs quantum wells in a GaAs cavity is ∼1.7 meV, while that reported by Camposeo *et al.*[57] for *J* aggregates of cyanine dye is about ∼35 meV. In contrast to these reports, the maximum TE-TM splitting in Fig. 7 is as large as ∼150 meV. Recently, a large TE-TM splitting of the same order of magnitude has been reported by Oda *et al.*[12] Although they did not clarify the origin of the large TE-TM splitting, it can be attributed to the plasmonic effects in the MIM structures.

In Fig. 7, we see that the TE-TM splitting in the empty microcavity has almost the same magnitude as that in the upper branch of the coupled modes. The very large TE-TM splitting presently observed for the upper branch can thus be attributed to the large TE-TM splitting in the empty microcavity arising from the plasmonic nature of the TM mode. Very recently, TE-TM splitting of the coupled modes less than 30 meV has been reported by Lodden and Holmes[14] for an organic layer bounded by Ag and Al mirrors. This cavity is also a hetero-MIM microcavity and can support a S-SPP mode. According to our calculation of the dispersion curves, the TE-TM splitting in the Ag-Al empty microcavity is much smaller than that in the Ag-Ag empty microcavity. This result well explains the smaller TE-TM splitting of the coupled modes in the doped Ag-Al microcavity. It is interesting to note here that relatively large TE-TM splitting of more than 40 meV has recently been reported by Bruückner *et al.*[58] for a system of a Ag thin film embedded in a DBR microcavity, which supports hybrid states of photonic modes and Tamm plasmons.[59] They could well reproduce their experimental results by using a transfer matrix method, which is an alternative approach to analyze the strong coupling.

D. Effects of optical anisotropy

As described in detail in the previous subsection, our fitting procedure yielded a value of E_{Rabi} for the TE-coupled mode (300 meV) slightly larger than that for the TM-coupled mode (280 meV). This difference in E_{Rabi} can be explained by the optical anisotropy in the TDBC-doped PVA film. In our experimental results, we found no appreciable sign of the optical anisotropy for PVA films not containing TDBC molecules. In fact, the experimental dispersion curves of the photonic modes in the empty MIM microcavity could be well reproduced by assuming an isotropic dielectric function (see Fig. 5). However, our TDBC-doped PVA films are thought to be optically anisotropic. As has been pointed out by Bonnand *et al.*[29] for their TDBC-doped PVA films very similar to ours, TDBC monomers are aggregated to form linear chains (*J* aggregates) and dispersed in the PVA matrix. During the spin coating process, the chains and their dipole moments tend to be aligned in the in-plane direction of the composite film. This anisotropic structure of the film induces the optical anisotropy.

Since the dipole moments of the *J* aggregates tend to be parallel to the film plane, the oscillator strength of the excitonic transition is larger in the in-plane direction than in the out-of-plane direction (uniaxial anisotropy). Therefore the interaction of excitons with the TE photonic mode, which has the electric field oriented in the in-plane direction, is stronger than with the TM photonic mode, which has the electric field inclined relative to the in-plane direction. Since E_{Rabi} in microcavities is known to be proportional to the square root of the oscillator strength of excitons, the value of E_{Rabi} presently obtained for the TE-coupled mode slightly larger than that for the TM-coupled mode can thus be well explained by the difference in the oscillator strength. It is very likely that TDBC-doped PVA films exhibit biaxial anisotropy reflecting the anisotropy in the film plane. In the case of the biaxial anisotropy, E_{Rabi} is expected to depend also on the direction of the in-plane wave vector. However, judging from the structure of the TDBC-doped PVA films, the anisotropy in the film plane is thought to be much smaller than the in-plane versus out-of-plane anisotropy. Therefore, the

variation in E_{Rabi} depending on the direction of the in-plane wave vector is expected to be much smaller than the difference in E_{Rabi} for the TE- and TM-coupled modes. In brief, although quantitative discussion is very difficult at present because of the lack of quantitative data on the optical anisotropy of the active layer, the present results can be well explained by assuming a constant E_{Rabi}, which is independent of the in-plane wave vector, but depends on the polarization.

It should be finally noted that the effects of the optical anisotropy in our experimental results are much smaller than the plasmonic effects. In fact, the amount of the TE-TM splitting in the upper branches of the coupled modes is as large as 150 meV and is of the same order of magnitude as the TE-TM splitting of the uncoupled modes in the empty microcavity. From the difference in the values of E_{Rabi} for the TE- and TM-coupled modes (20 meV), the contribution of the optical anisotropy to the observed TE-TM splitting of the coupled modes is estimated to be of the order of a few tens of meV. Therefore the conclusions drawn for the plamonic effects in the previous subsections are unchanged. Further detailed experimental and theoretical studies are required to perform quantitative analyses of the effects of the optical anisotropy. It may be of prime importance to determine the dielectric tensor for the TDBC-doped PVA film, which is believed to have a biaxial symmetry. It is also necessary to develop theoretical calculations that allow us to obtain dispersion curves of plasmonic modes supported by the MIM microcavity with an optically anisotropic insulator layer.

IV. CONCLUSION

We prepared MIM microcavities consisting of a PVA layer doped and undoped with J aggregates of TDBC molecules sandwiched by 35-nm thick Ag mirrors. Reflection and transmission spectra of the samples were measured with s- and p-polarized incident light for various incident angles. The undoped-MIM sample exhibited a single reflection dip and a single transmission peak for a given incident angle. Dispersion curves determined from the reflection data are in good agreement with those calculated from power dissipation spectra of an oscillating dipole located in the microcavity. From the good agreement, the photonic modes supported by the undoped-MIM microcavity could be assigned unambiguously to the TE_0 and S-SPP modes. The S-SPP mode is a TM mode of plasmonic origin that arises from the coupling of SPP modes at two metal-insulator interfaces in the microcavity. The doped-MIM sample exhibited doublets of reflection dips and transmission peaks, which are the consequences of strong coupling between excitons in the J aggregates and photonic modes supported by the MIM cavity. Dispersion curves of the TE- and TM-coupled modes determined from the reflection data could be well reproduced by a standard expression of the coupled-mode dispersion by using dispersion curves of the TE_0 and S-SPP modes in the empty microcavity. A small difference in the values of the Rabi splitting energy for the TE- and TM-coupled modes can be attributed to the optical anisotropy of the TDBC-doped PVA film.

Although Oda *et al.*[12] had difficulty in reproducing the TM-coupled mode in their Ag-Ag microcavity similar to ours based on the theory of photonic modes in the DBR microcavity, the present results demonstrate that there is no such difficulty when the plasmonic nature of the TM mode in the empty microcavity is appropriately taken into account. The TE-TM splitting in the upper branch of the coupled mode found in our dispersion curves is extremely large compared with those previously reported for DBR microcavities. The large splitting can also be well explained by the behavior of the S-SPP mode in the Ag-Ag empty microcavity. The contribution of the optical anisotropy of the active film to the observed TE-TM splitting is estimated to be much smaller than that of the plasmonic effects. To our knowledge, the plasmonic effects have not been taken into account appropriately in analyzing experimental results on the strong coupling in MIM microcavities. The present results demonstrate the importance of the plasmonic effects to consistently interpret the experimental data. The present results may also be of practical importance in developing photonic devices based on the strong exciton-photon coupling in MIM microcavities.

ACKNOWLEDGMENTS

This work was supported in part by a Grant-in-Aid for Scientific Research (B) (No.23310064) from JSPS and that on Priority Area, "Strong Photon-Molecule Coupling Fields" (No. 470) from MEXT, Japan.

*hayashi@eedept.kobe-u.ac.jp

[1] M. S. Skolnick, T. A. Fisher, and D. M. Whittaker, Semicond. Sci. Tech. **13**, 645 (1998).

[2] G. Panzarini, L. C. Andreani, A. Armitage, D. Baxter, M. S. Skolnick, V. N. Astratov, J. S. Roberts, A. V. Kavokin, M. R. Vladimirova, and M. A. Kaliteevski, Phys. Solid State **41**, 1223 (1999).

[3] R. Houdré, Phys. Status Solidi B **242**, 2167 (2005).

[4] B. Deveaud, *The Physics of Semiconductor Microcavities* (WILEY-VCH, Weinheim, 2007).

[5] R. J. Holmes and S. R. Forrest, Org. Electron. **8**, 77 (2007).

[6] H. M. Gibbs, G. Khitrova, and S. W. Koch, Nat. Photon. **5**, 275 (2011).

[7] C. Weisbuch, N. Nishioka, A. Ishikawa, and Y. Arakawa, Phys. Rev. Lett. **69**, 3314 (1992).

[8] D. G. Lidzey, D. D. C. Bradley, M. S. Skolnick, T. Virgili, S. Walker, and D. M. Whittaker, Nature (London) **395**, 53 (1998).

[9] D. G. Lidzey, D. D. C. Bradley, T. Virgili, A. Armitage, M. S. Skolnick, and S. Walker, Phys. Rev. Lett. **82**, 3316 (1999).

[10] P. A. Hobson, W. L. Barnes, D. G. Lidzey, G. A. Gehring, D. M. Whittaker, M. S. Skolnick, and S. Walker, Appl. Phys. Lett. **81**, 3519 (2002).

[11] J. R. Tischler, M. S. Bradley, V. Bulovic, J. H. Song, and A. Nurmikko, Phys. Rev. Lett. **95**, 036401 (2005).

[12] M. Oda, K. Hirata, T. Inoue, Y. Obara, T. Fujimura, and T. Tani, Phys. Status Solidi C **6**, 288 (2009).

[13]T. Schwartz, J. A. Hutchison, C. Genet, and T. W. Ebbesen, Phys. Rev. Lett. **106**, 196405 (2011).
[14]G. H. Lodden and R. A. Holmes, Appl. Phys. Lett. **98**, 233301 (2011).
[15]C. Ciuti, G. Bastard, and I. Carusotto, Phys. Rev. B **72**, 115303 (2005).
[16]S. De Liberato, C. Ciuti, and I. Carusotto, Phys. Rev. Lett. **98**, 103602 (2007).
[17]Y. Todorov, A. M. Andrews, R. Colombelli, S. De Liberato, C. Ciuti, P. Klang, G. Strasser, and C. Sirtori, Phys. Rev. Lett. **105**, 196402 (2010).
[18]A. A. Anappara, S. De Liberato, A. Tredicucci, C. Ciuti, G. Biasiol, L. Sorba, and F. Beltram, Phys. Rev. B **79**, 201303(R) (2009).
[19]G. Günter, A. A. Anappara, J. Hees, A. Sell, G. Biasiol, L. Sorba, S. De Liberato, C. Ciuti, A. Tredicucci, A. Leitenstorfer, and R. Huber, Nature (London) **458**, 178 (2009).
[20]T. Niemczyk, F. Deppe, H. Huebl, E. P. Menzel, F. Hocke, M. J. Schwarz, J. J. Garcia-Ripoll, D. Zueco, T. Hümmer, E. Solano, A. Marx, and R. Gross, Nat. Phys. **6**, 772 (2010).
[21]V. M. Agranovich and A. G. Malshukov, Opt. Commun. **11**, 169 (1974).
[22]V. M. Agranovich, S. A. Darmanyan, and A. G. Mal'chukov, Opt. Commun. **33**, 234 (1980).
[23]V. M. Agranovich and D. L. Mills, *Surface Polaritons* (North-Holland, Amsterdam, 1982).
[24]V. G. Yakovlev, V. A. Nazin, and G. N. Zhizhin, Opt. Commun. **15**, 293 (1975).
[25]T. Lopez-Rios, F. Abelès, and G. Vuye, J. Phys. **39**, 645 (1978).
[26]I. Pockrand, A. Brillante, and D. Möbius, J. Chem. Phys. **77**, 6289 (1982).
[27]J. Bellessa, C. Bonnand, J. C. Plenet, and J. Mugnier, Phys. Rev. Lett. **93**, 036404 (2004).
[28]J. Dintinger, S. Klein, F. Bustos, W. L. Barnes, and T. W. Ebbesen, Phys. Rev. B **71**, 035424 (2005).
[29]C. Bonnand, J. Bellessa, and J. C. Plenet, Phys. Rev. B **73**, 245330 (2006).
[30]D. E. Gomez, K. C. Vernon, P. Mulvaney, and T. J. Davis, Nano Lett. **10**, 274 (2010).
[31]A. Berrier, R. Cools, C. Arnold, P. Offermans, M. Crego-Calama, S. H. Brongersma, and J. Gomez-Rivas, Acs Nano **5**, 6226 (2011).
[32]N. I. Cade, T. Ritman-Meer, and D. Richards, Phys. Rev. B **79**, 241404 (R) (2009).
[33]J. Bellessa, C. Symonds, A. Vynck, K.and Lemaitre, A. Brioude, L. Beaur, J. C. Plenet, P. Viste, D. Felbacq, E. Cambril, and P. Valvin, Phys. Rev. B **80**, 033303 (2009).
[34]D. D. Lekeufack, A. Brioude, A. W. Coleman, P. Miele, J. Bellessa, L. D. Zeng, and P. Stadelmann, Appl. Phys. Lett. **96**, 253107 (2010).
[35]E. N. Economou, Phys. Rev. **182**, 539 (1969).
[36]W. L. Barnes, J. Lightwave Technol. **17**, 2170 (1999).
[37]F. Villa, T. Lopez-Rios, and L. E. Regalado, Phys. Rev. B **63**, 165103 (2001).
[38]J. A. Dionne, L. A. Sweatlock, H. A. Atwater, and A. Polman, Phys. Rev. B **73**, 035407 (2006).
[39]F. Kusunoki, T. Yotsuya, and J. Takahara, Opt. Express. **14**, 5651 (2006).
[40]H. T. Miyazaki and Y. Kurokawa, Phys. Rev. Lett. **96**, 097401 (2006).
[41]L. H. Smith, M. C. Taylor, I. R. Hooper, and W. L. Barnes, J. Mod. Opt., **55**, 2929 (2008).
[42]S. I. Bozhevolnyi, *Plasmonic Nanoguides and Circuits* (Pan Stanford Publishing, Singapore, 2009).
[43]D. Y. Lei and H. C. Ong, Appl. Phys. Lett. **91**, 211107 (2007).
[44]J. Feng, T. Okamoto, J. Simonen, and S. Kawata, Appl. Phys. Lett. **90**, 081106 (2007).
[45]S. Hayashi, A. Maekawa, S. C. Kim, and M. Fujii, Phys. Rev. B **82**, 035441 (2010).
[46]A. A. Bogdanov and R. A. Suris, Phys. Rev. B **83**, 125316 (2011).
[47]M. Litinskaya and V. M. Agranovich, J. Phys.: Condens. Matter **24**, 015302 (2012).
[48]H. Becker, N. Burns, N. Tessler, and R. Friend, J. Appl. Phys. **81**, 2825 (1997).
[49]F. Ma and X. Liu, Appl. Opt. **46**, 6247 (2007).
[50]M. van Burgel, D. A. Wiersma, and K. Duppen, J. Chem. Phys. **102**, 20 (1995).
[51]W. L. Barnes, J. Mod. Opt. **45**, 661 (1998).
[52]R. R. Chance, A. Prock, and R. Silbey, Adv. Chem. Phys. **37**, 1 (1978).
[53]E. D. Palik, *Handbook of Optical Constants of Solids* (Academic, Orlando, 1985).
[54]M. Yoshida, S. Tomita, H. Yanagi, and S. Hayashi, Phys. Rev. B **82**, 045410 (2010).
[55]Y. Wang, Appl. Phys. Lett. **82**, 4385 (2003).
[56]V. M. Agranovich, M. Litinskaia, and D. G. Lidzey, Phys. Rev. B **67**, 085311 (2003).
[57]A. Camposeo, L. Persano, P. Del Carro, T. Virgili, R. Cingolani, and D. Pisignano, Org. Electron. **8**, 114 (2007).
[58]R. Brückner, M. Sudzius, S. I. Hintschich, H. Fröb, V. G. Lyssenko, M. A. Kaliteevski, I. Iorsh, R. A. Abram, A. V. Kavokin, and K. Leo, Appl. Phys. Lett. **100**, 062101 (2012).
[59]M. Kaliteevski, I. Iorsh, S. Brand, R. A. Abram, J. M. Chamberlain, A. V. Kavokin, and I. A. Shelykh, Phys. Rev. B **76**, 165415 (2007).